The QCD Phase Transition with Two Quark Flavours

C. Czaban, F. Cuteri, O. Philipsen, C. Pinke, A. Sciarra

published in

NIC Symposium 2016
K. Binder, M. Müller, M. Kremer, A. Schnurpfeil (Editors)

Forschungszentrum Jülich GmbH,
John von Neumann Institute for Computing (NIC),
Schriften des Forschungszentrums Jülich, NIC Series, Vol. 48,
ISBN 978-3-95806-109-5, pp. 31.
http://hdl.handle.net/2128/9842

The QCD Phase Transition with Two Quark Flavours

Christopher Czaban[1,2], **Francesca Cuteri**[1], **Owe Philipsen**[1,2], **Christopher Pinke**[1], **and Alessandro Sciarra**[1,2]

[1] Institut für Theoretische Physik, Goethe Universität Frankfurt,
Max-von-Laue-Str. 1, 60438 Frankfurt, Germany
E-mail: {czaban, cuteri, philipsen, pinke, sciarra}@th.physik.uni-frankfurt.de

[2] John von Neumann Institute for Computing (NIC), GSI, Planckstr. 1, 64291 Darmstadt, Germany

The QCD phase diagram, specifying the form of strongly interacting matter as a function of temperature and density, is important in many disciplines of physics. Finite densities are not amenable to standard Monte Carlo simulations and knowledge of the phase diagram remains scarce. We report from a long term project to determine the phase diagram of QCD with two mass degenerate quark species at zero and imaginary chemical potential, where there is no sign problem, in order to constrain the phase diagram of physical QCD at real chemical potential.

1 Introduction

The fundamental theory of the strong interactions governing the forces between nuclear and subnuclear particles is Quantum Chromodynamics (QCD). Its fundamental degrees of freedom are light u- and d-quarks, a heavier s-quark and gluons. A key feature of the theory is asymptotic freedom with the coupling strength depending on the energy scale of a scattering process. For energies below a few GeV, the coupling is large and quarks and gluons combine into numerous tightly bound states, the hadrons, among them the familiar nucleons proton and neutron. On the other hand, at large temperatures or densities, the average energy per particle is higher and the theory enters a weak coupling regime, where the quarks and gluons form a plasma. The QCD phase diagram determines the form of matter under different conditions as a function of temperature, T, and chemical potential for baryon number, μ_B, as sketched in Fig. 1. Whether and where these regions are separated

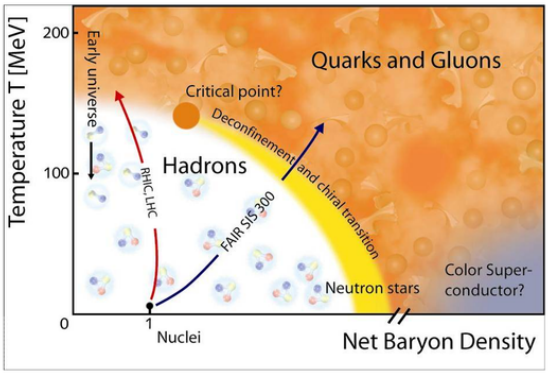

Figure 1. The QCD phase diagram as a function of temperature and chemical potential for baryon density.

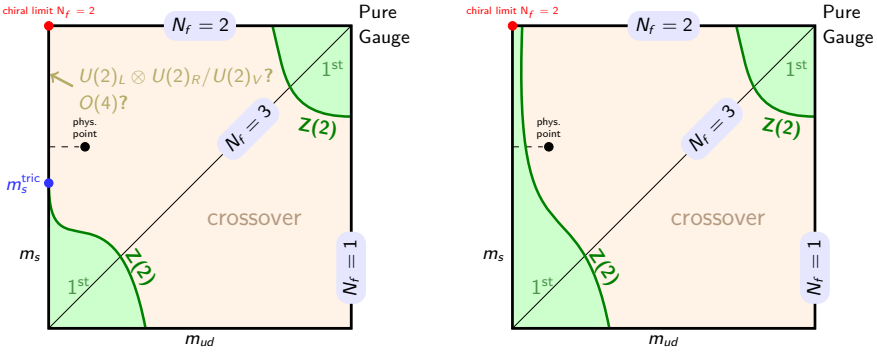

Figure 2. Possible scenarios for the QCD phase diagram at $\mu = 0$ as function of quark mass.

by true phase transitions has to be determined by first principle calculations and experiments. Since QCD is strongly coupled on scales of hadronic matter, a non-perturbative treatment is necessary and Monte Carlo simulations of lattice QCD are the only fully reliable approach. Unfortunately, the so-called sign problem prohibits straightforward simulations at finite baryon density. There are several approximate ways to circumvent this problem, all of them valid for $\mu/T \lesssim 1$ only[1] (with quark chemical potential $\mu = \mu_B/3$). On the other hand, at imaginary chemical potential there is no sign problem. Results from such simulations can be either analytically continued after fitting to power series, or used as a way to constrain the phase diagram at zero and real μ.

The order of the finite temperature phase transition at zero density depends on the quark masses and is schematically shown in Fig. 2 (left), where N_f denotes the number of mass degenerate quark flavours. In the limits of zero and infinite quark masses (lower left and upper right corners), order parameters corresponding to the breaking of a global symmetry can be defined, and for three degenerate quarks one numerically finds first order phase transitions at small and large quark masses at some finite temperatures $T_c(m)$. On the other hand, one observes an analytic crossover at intermediate quark masses, with second order boundary lines separating these regions. Both lines have been shown to belong to the $Z(2)$ universality class of the 3d Ising model[2–4]. The critical lines bound the quark mass regions featuring a chiral or deconfinement phase transition, and are called chiral and deconfinement critical lines, respectively. The former has been mapped out on $N_\tau = 4$ lattices[5] and puts the physical quark mass configuration in the crossover region. The chiral critical line recedes with decreasing lattice spacing[6,7]: for $N_f = 3$, on the critical point $m_\pi(N_\tau = 4)/m_\pi(N_\tau = 6) \sim 1.8$. Thus, in the continuum the physical point is deeper in the crossover region than on coarse lattices.

An open question to this day remains the order of the transition in the limit of zero light quark masses, called the chiral limit. As explained below, this limit cannot be directly simulated. Consequently, it is still not known whether the chiral phase transition for two quark flavours is of first or second order. Hence an alternative scenario is Fig. 2 (right). Clarifying this question is important because of the proximity of the critical line to the physical point.

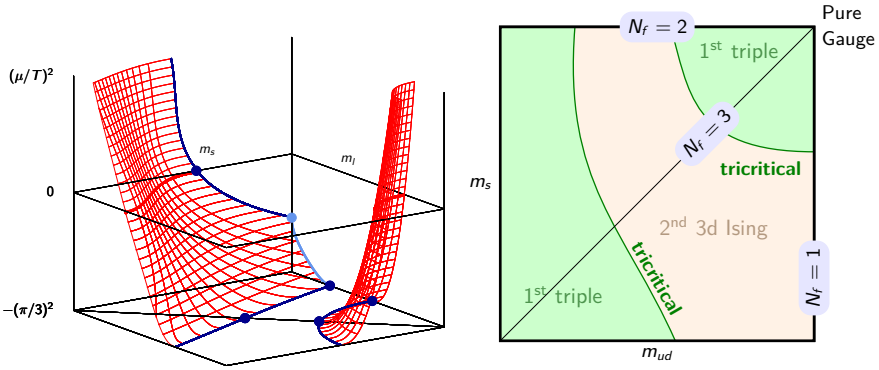

Figure 3. Left: As Fig. 2 with an additional axis for quark chemical potential. Right: Bottom plane of the left.

2 Imaginary Chemical Potential

At imaginary chemical potential $\mu = i\mu_i$ the sign problem is absent and standard simulation algorithms can be applied. Because of an exact symmetry $Z(\mu) = Z(-\mu)$, the partition function is a function of μ^2. We can then plot Fig. 2 with a third axis, Fig. 3 (left). The chiral and deconfinement critical lines now become critical surfaces as functions of μ^2, with analytic continuations between real and imaginary μ. The curvature of the chiral critical surface has been computed[8]. In this region of phase space, there is an exact periodic (Roberge-Weiss (RW)) symmetry[9],

$$Z\left(\mu\right) = Z\left(\mu + 2\pi ik/3\right),\ k \in \mathbb{N}\,, \tag{1}$$

with critical values of $\mu_i^c = (2k+1)\pi/3, (k \in \mathbb{N})$, marking boundaries between adjacent centre sectors of the $SU(3)$ gauge group of QCD. The first boundary constitutes the bottom of Fig. 3 (left) and is shown separately in Fig. 3 (right). First order transition regions for light and heavy quarks are bounded by tricritical lines on which the critical surfaces terminate[10]. Note that at this value of imaginary chemical potential, the first order region for two light quark flavours is large enough so that it can actually be seen in simulations on $N_\tau = 4, 6$. In this work, we compute the positions of the tricritical points on the upper $N_f = 2$ line in that diagram on finer $N_\tau = 6$ lattices using Wilson fermions. We also map out the boundary line of the chiral critical surface in the $N_f = 2$ plane on $N_\tau = 4$ lattices.

3 Simulating Thermodynamical Systems in Lattice QCD

The central object in statistical physics is the partition function $\mathcal{Z}$ of a system. For lattice QCD it is expressed as a path integral over the gluon fields U, including a determinant of the Dirac operator for the quarks. An expectation value of some observable A then reads

$$\langle A \rangle = \mathcal{Z}^{-1} \int \mathcal{D}U\, A \det D[U] \exp\left\{-S_g[U]\right\}\ . \tag{2}$$

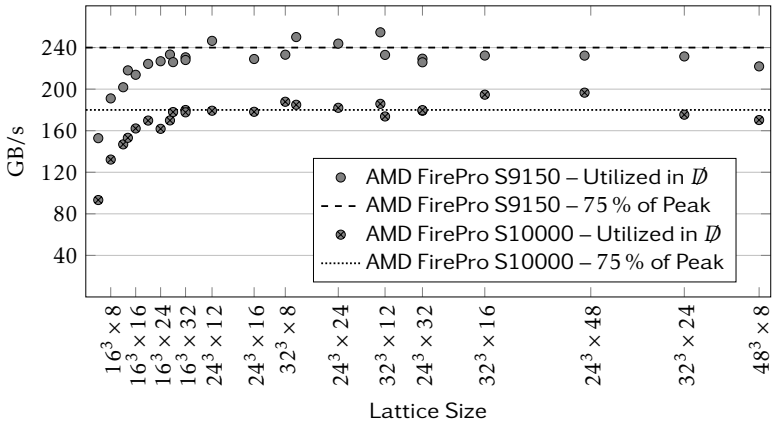

Figure 4. Benchmark of $\not{D}$ for the L-CSC GPUs (taken from Ref. 14).

For our study we used the standard Wilson gauge action $S_g[U]$ as well as the standard Wilson Dirac operator $D[U]$, for detailed expressions see Ref. 11.

The bare parameters are the lattice gauge coupling $\beta = 6/g^2$, and the bare quark mass $m_{u,d} \equiv m$, which is encoded in the hopping parameter κ

$$\kappa = \frac{1}{2(a\,m + 4)} \; .$$

A finite temperature T is specified by the inverse spatial lattice extent

$$T = (a(\beta) N_\tau)^{-1} \; . \tag{3}$$

On a lattice with given N_τ, temperature is tuned by changing the lattice spacing a indirectly via the running coupling $\beta(a)$. On the other hand, a continuum limit at fixed temperature implies $a \to 0, N_\tau \to \infty$, and larger values of N_τ imply smaller lattice spacings.

The determinant of the fermion matrix D is expressed in terms of pseudo fermions ϕ,

$$\det D[U] \sim \int \mathcal{D}\phi^\dagger \, \mathcal{D}\phi \exp\left\{-\phi^\dagger D^{-1}[U]\phi\right\} \; , \tag{4}$$

yielding the effective action $S_{\text{eff}}[U,\phi] = S_{\text{gauge}}[U] + \phi^\dagger D^{-1}[U]\phi$. Importance sampling methods are used to evaluate this high-dimensional integral. Using the Boltzmann-weight $p[U,\phi] = \exp\{-S_{\text{eff}}[U,\phi]\}$ as probability measure, an ensemble of N gauge configurations $\{U_m\}$ is generated. Then, $\langle A \rangle$ may be approximated by

$$\langle A \rangle \approx \frac{1}{N} \sum_m A[U_m] \; . \tag{5}$$

The standard simulation algorithm to generate QCD gauge configurations is the Hybrid Monte-Carlo (HMC) algorithm, where the effective action is embedded in a fictitious classical system evolved over a time τ according to the Hamiltonian equations of motion.

Since the fermion matrix D is high-dimensional and sparse, iterative Krylov space methods are used. D^{-1} is calculated indirectly out of equations like

$$D\phi = \psi \Rightarrow \phi = D^{-1}\psi \; . \tag{6}$$

This inversion is the most cost-intensive part of a simulation. Thus, for performance it is crucial to have a well tuned implementation, in particular of the derivative term $\not{D}$. The numerical costs for the HMC scales like $V^{5/4}$ and m_π^{-6}. This illustrates that LQCD studies are very cost-intensive, especially when going towards the chiral limit, and efficient simulation programs are needed. We thermalised configurations on JUQUEEN. For production we employed our publicly available[a] OpenCL[b]-based code CL^{2}QCD[12], which is optimised to run efficiently on the GPUs of the LOEWE-CSC[13] at Goethe-University Frankfurt and the L-CSC[14] at GSI in Darmstadt. The latter was recently ranked as the most energy efficient computing cluster in the world[c]. Fig. 4 shows the performance of the $\not{D}$ on this cluster and underlines the efficient implementation.

4 Identifying Phase Transitions

	Crossover	1^{st} triple	Tricritical	$3D$ Ising
B_4	3	1.5	2	1.604
ν	–	$1/3$	$1/2$	0.6301(4)
γ	–	1	1	1.2372(5)

Table 1. Critical values of ν, γ and $B_4 \equiv B_4(X, \alpha_c)$ for the universality classes needed here[16].

In order to identify the phase transition as a function of the QCD parameters, we use the Binder cumulant[15] defined as

$$B_4(X, \alpha_1, \ldots, \alpha_n) \equiv \frac{\left\langle (X - \langle X \rangle)^4 \right\rangle}{\left\langle (X - \langle X \rangle)^2 \right\rangle^2} ,$$

where X is a general observable and $\alpha_1, \ldots, \alpha_n$ is a set of parameter on which B_4 depends. Our observables are the Polyakov loop and the chiral condensate, and the QCD parameters are $\{\alpha_i\} = \{\beta, \kappa, \mu_i\}$. First we find the location of phase transitions by the vanishing third moment of the fluctuations in the observables, $\langle (X - \langle X \rangle)^3 \rangle \approx 0$, for critical parameter sets α_i^c. The nature of the transition then has to be extracted from finite size scaling on those parameter values. Non-analytic phase transitions only exist in the thermodynamic limit $V \to \infty$, for which the Binder cumulant takes different values depending on the nature of the phase transition (see Tab. 1). Even though B_4 is a non-analytic step function for $V \to \infty$, at finite volume it gets smoothed out and its slope increases with the volume. Around the critical coupling β_c, the Binder cumulant is a function of $x \equiv (\beta - \beta_c) N_\sigma^{1/\nu}$ only and can be Taylor-expanded around 0. The first finite-size corrections are

$$B_4(\beta, N_\sigma) = B_4(\beta_c, \infty) + a_1\, x + a_2\, x^2 + \mathcal{O}(x^3) . \tag{7}$$

[a] See `github.com/CL2QCD/` .

[b] See `www.khronos.org/opencl` for more information.

[c] See `http://www.green500.org/news/green500-list-november-2014` .

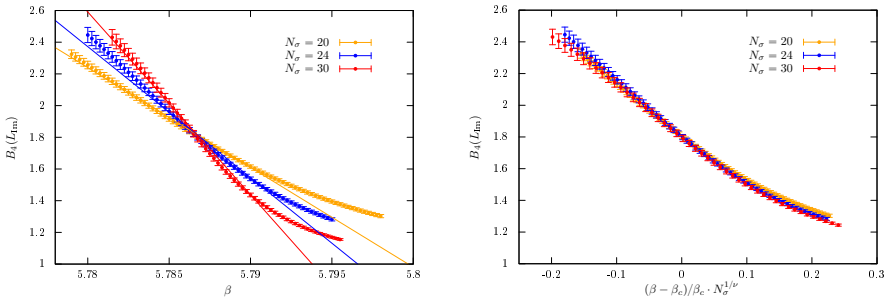

Figure 5. Binder cumulant for $\kappa = 0.13$ and $N_\tau = 6$. Left: Reweighted data including linear fits. Right: Collapse plot with second order exponents.

Close to the thermodynamic limit, the intersection of different curves from different volumes gives β_c and the critical exponent ν takes its value depending on the type of transition. While the value of the Binder cumulant is very sensitive to finite size corrections and in some cases not close to its infinite volume value, the exponents are more stable.

Our strategy to locate the two tricritical values of κ is described in detail in Ref. 17. For each simulated quark mass parametrised by κ, we measured the Binder cumulant around the critical coupling β_c and extracted the value of ν fitting our data according to Eq. 7. Because of the particularly delicate fitting procedure required to extract the critical exponent ν from Eq. 7, we usually produced four different Markov chains for each value of the coupling in order to acquire statistics in a faster manner and also to better understand if the collected statistics was enough. Ferrenberg-Swendsen reweighting[18] was used to produce additional β-points and thus to smooth the data. An example is shown in Fig. 5 (left). We then check the consistency of our fitted exponents by replotting the data with the nearest exact critical exponent. To the extent that the data are correctly described by these exponents, they collapse onto a universal curve in the neighbourhood of the critical coupling as in Fig. 5 (right).

5 Results

Fig. 6 shows the critical exponents ν for QCD with two flavours of Wilson quarks simulated at $\mu_i = \pi T/3$ as a function of hopping parameter and thus quark masses on $N_\tau = 4$ (left)[17] and $N_\tau = 6$ (right) lattices. We clearly observe the change from a first order behaviour to second order values and back, passing through tricritical points. These correspond to the tricritical points on the upper boundary of Fig. 3 for two different lattice spacings. As is the case for $\mu = 0$, the chiral first order region is shrinking with growing N_τ, i.e. as the lattice gets finer. Additional finer lattice spacings are required in future simulations before extrapolations to the continuum can be undertaken and conclusions can be drawn.

In a second set of calculations we have mapped out the critical boundary line in the $N_f = 2$ backplane of Fig. 3 (left)[19], following a recent suggestion to allow for a determination of the nature of the chiral phase transition at $\mu = 0$[20]. The situation and its particular interest are shown in Fig. 7 (left). The boundary line coming from the tricritical point at $\mu_i = \pi T/3$ has to terminate in another tricritical point on the μ^2-axis. If the line hits the

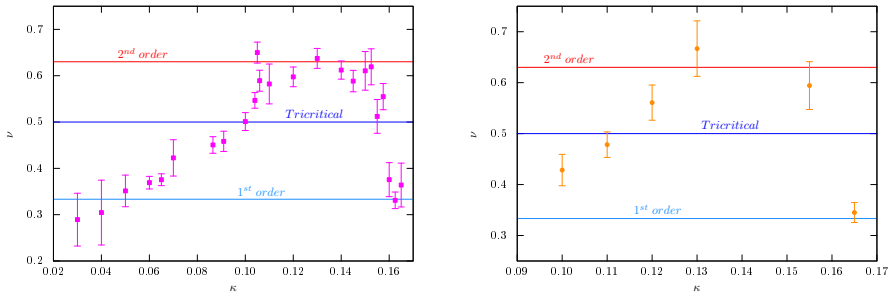

Figure 6. Critical exponents in the RW plane as a function of mass for $N_\tau = 4$ (left) and $N_\tau = 6$ (right).

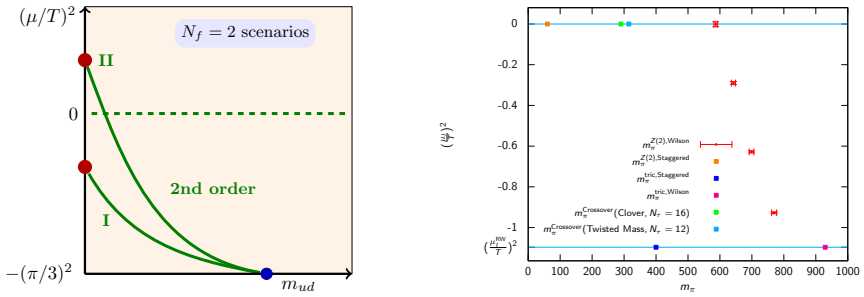

Figure 7. Left: Possibilities for the boundary of the chiral critical surface in the $N_f = 2$ backplane of Fig. 3 (left). To the left of the lines is first order region, to the right crossover. Right: The boundary line for $N_\tau = 4$.

axis at $\mu < 0$, the chiral phase transition at $\mu = 0$ is of second order, whereas if it hits at $\mu > 0$ there is a first order region around the chiral limit. The boundary line is in the 3D Ising universality class and we can again use the Binder cumulant to identify and map it out. Fig. 7 (right) shows the results of our simulations. Note that, in order to be able to compare different lattice spacings as well as different lattice discretisation, the horizontal axis of the figure is the pion mass rather than κ or the quark mass. This is because the quark mass receives renormalisation factors specific to a particular choice of discretisation, whereas the pion mass is a renormalisation group invariant physical quantity, that directly depends on κ and can be compared between different lattice discretisations.

The figure illustrates that Wilson fermions on coarse lattices clearly feature a large region of first order chiral transitions. Note that this region is much larger than in the case of staggered fermions, which are also shown. This difference must be due to discretisation effects, since the physics in the continuum must be independent of the discretisation scheme chosen. One may speculate that the Wilson results have the larger discretisation effects, since there are already simulations with improved Wilson actions at smaller lattice pion masses which are in the crossover region. The huge discrepancies illustrate the need to go to much finer lattices, and hence require significantly more High Performance Computing time, before any conclusions for the continuum can be drawn.

6 Summary

We have started a systematic investigation of the phase structure of QCD with two flavours of standard Wilson fermions at zero and imaginary chemical potentials. On coarse lattices we find clear evidence for a first order chiral phase transition. However, comparison between different lattice spacings and different discretisation schemes shows huge discretisation artefacts. These have to be removed by future simulations on much finer lattices in order to draw conclusions for continuum physics. This highlights the continued and growing need for High Performance Computing in elementary particle and nuclear physics.

Acknowledgements

C.C., C. P. and A.S. were supported by the Helmholtz International Center for FAIR and HGS-Hire within the LOEWE program of the State of Hesse, O.P. was supported by BMBF grant 06FY7100. The authors thank the administrating teams of LOEWE-CSC at GU, L-CSC at GSI and JUQUEEN at NIC.

References

1. P. de Forcrand, PoS **LAT2009** (2009) 010 [arXiv:1005.0539 [hep-lat]].
2. F. Karsch, E. Laermann and C. Schmidt, Phys. Lett. B **520** (2001) 41 [arXiv:hep-lat/0107020].
3. P. de Forcrand and O. Philipsen, Nucl. Phys. B **673** (2003) 170 [arXiv:hep-lat/0307020].
4. S. Kim *et al.*, PoS **LAT2005**, (2006) 166 [arXiv:hep-lat/0510069].
5. P. de Forcrand and O. Philipsen, JHEP **0701** (2007) 077 [hep-lat/0607017].
6. P. de Forcrand, S. Kim and O. Philipsen, PoS **LAT2007** (2007) 178 [arXiv:0711.0262 [hep-lat]].
7. G. Endrődi *et al.*, PoS **LAT2007** (2007) 182 [arXiv:0710.0998 [hep-lat]].
8. P. de Forcrand and O. Philipsen, JHEP **0701** (2007) 077 [hep-lat/0607017].
9. A. Roberge and N. Weiss, Nucl. Phys. B **275** (1986) 734.
10. P. de Forcrand and O. Philipsen, Phys. Rev. Lett. **105** (2010) 152001 [arXiv:1004.3144 [hep-lat]].
11. C. Gattringer and C. B. Lang, Lect. Notes Phys. **788** (2010) 1.
12. M. Bach, V. Lindenstruth, O. Philipsen and C. Pinke, Comput. Phys. Commun. **184** (2013) 2042 [arXiv:1209.5942 [hep-lat]].
13. M. Bach *et al.*, Computer Science - Research and Development **26** (2011).
14. D. Rohr, M. Bach, G. Neskovic, V. Lindenstruth, C. Pinke and O. Philipsen, High Performance Computing LNCS **9137** (2015).
15. K. Binder, Z. Phys. B **43** (1981) 119.
16. A. Pelissetto and E. Vicari, Phys. Rept. **368** (2002) 549 [cond-mat/0012164].
17. O. Philipsen and C. Pinke, Phys. Rev. D **89** (2014) [arXiv:1402.0838 [hep-lat]].
18. A. M. Ferrenberg and R. H. Swendsen, Phys. Rev. Lett. **63** (1989) 1195.
19. O. Philipsen, C. Pinke, PoS **LAT2015** (2015) 149, [arXiv:1508.07725 [hep-lat]].
20. C. Bonati, P. de Forcrand, M. D'Elia, O. Philipsen and F. Sanfilippo, Phys. Rev. D **90** (2014) 7, 074030 [arXiv:1408.5086 [hep-lat]].